Adsorption-desorption processes of polydisperse mixtures on a triangular lattice

D. Dujak,[1] I. Lončarević,[2] Lj. Budinski-Petković,[2] S. B. Vrhovac,[3,*] and A. Karač[1]

[1]*Faculty of Metallurgy and Materials, University of Zenica, Bosnia and Herzegovina*
[2]*Faculty of Engineering, Trg D. Obradovića 6, Novi Sad 21000, Serbia*
[3]*Institute of Physics, P.O. Box 68, Zemun 11080, Belgrade, Serbia*

Adsorption-desorption processes of polydisperse mixtures on a triangular lattice are studied by numerical simulations. Mixtures are composed of the shapes of different numbers of segments and rotational symmetries. Numerical simulations are performed to determine the influence of the number of mixture components and the length of the shapes making the mixture on the kinetics of the deposition process. We find that, above the jamming limit, the time evolution of the total coverage of a mixture can be described by the Mittag-Leffler function $\theta(t) = \theta_\infty - \Delta\theta E_\beta[-(t/\tau)^\beta]$ for all the mixtures we have examined. Our results show that the equilibrium coverage decreases with the number of components making the mixture and also with the desorption probability, via corresponding stretched exponential laws. For the mixtures of equal-sized objects, we propose a simple formula for predicting the value of the steady-state coverage fraction of a mixture from the values of the steady-state coverage fractions of pure component shapes.

I. INTRODUCTION

Adsorption of extended particles on various surfaces is involved in a large variety of physical, chemical, and biological processes. Deposition processes in which the events occur essentially irreversibly on the time scales of the experiment can be studied as random sequential adsorption (RSA) [1–3].

In the RSA model objects of a specified shape are randomly and sequentially deposited onto a substrate without overlapping each other. The adsorbed particles are permanently fixed at their spatial positions and they affect the geometry of all later placements. The kinetic properties of a deposition process are described by the evolution of the coverage $\theta(t)$, which is the fraction of the substrate area covered by the adsorbed particles. The deposition process ceases when all unoccupied spaces are smaller than the size of an adsorbing object. The system is then jammed in a disordered state for which the limiting (jamming) coverage θ_{jam} is less than that in the close packing. Depending on the system of interest, the substrate can be continuum or discrete and RSA models can differ in substrate dimensionality. Jamming coverage depends on the shape and on the size of the depositing objects. An asymptotic approach of the coverage fraction $\theta(t)$ to its jamming limit follows a power law [4,5] for continuum systems, while in the case of lattice deposition models the approach to the jamming limit is exponential with the rate dependent mostly on the symmetry properties of the object [6,7].

In real physical situations, however, one often needs to consider the possibility of desorption or diffusion of deposited particles. Examples of such processes are catalytic reactions, binding of motor proteins to microtubules in living cells [8], etc. Compaction of granular materials can also be successfully modeled using adsorption-desorption processes which reproduce the slow density relaxation [9,10], memory effects [11,12], and other features of vibrated granular materials. The dynamics of the reversible RSA model depends on the excluded volume and geometrical frustration, just as in the case of granular compaction. This model can be regarded as a simple picture of a horizontal layer of a granular material, perpendicular to the tapping force. As a result of a tapping event, particles leave the layer at random and compaction proceeds when particles fall back into the layer under the influence of gravity. The ratio of desorption to adsorption probability within the model plays a role of vibration intensity.

Allowing desorption makes the process reversible and the system ultimately reaches an equilibrium state. Adsorption-desorption processes in one dimension were studied analytically [13] and an exact solution for the equilibrium properties was obtained. Steady-state density was found to be a function only of the adsorption to desorption rate ratio. Continuum adsorption-desorption models display a three-stage approach of the coverage to its equilibrium value: an algebraic one where the coverage varies as $1/t$ and a logarithmic one where the coverage varies as $1/\ln(t)$, followed by a terminal exponential approach [9,14,15]. On one-dimensional lattice a power-law decay of the density of interparticle gaps in a time range after the initial "jamming" was obtained [16]. Numerical simulations of reversible lattice deposition suggested that kinetics of the process depends on the dimensionality of the system. For adsorption-desorption processes of k-mers on a one-dimensional lattice [17,18] it was found that a stretched exponential growth of the coverage $\theta(t)$ toward the steady-state value θ_{eq} occurs: $\theta_{\text{eq}} - \theta(t) \propto \exp[-(t/\tau)^\beta]$. On the other hand, results of the numerical simulations of reversible RSA on a triangular lattice obtained for a wide variety of object shapes [10] showed an excellent agreement of the relaxation dynamics with the function of the form:

$$\theta(t) = \theta_\infty - \Delta\theta\, E_\beta(-(t/\tau)^\beta), \quad \Delta\theta = \theta_{\text{eq}} - \theta_0, \quad (1)$$

where θ_∞, θ_0, τ, and β are the fitting parameters and E_β denotes the Mittag-Leffler function of order β [19]. Note that the Mittag-Leffler function is one of the most frequently used phenomenological fitting functions for relaxation processes in many complex disordered systems such as glasses,

_____
*vrhovac@ipb.ac.rs; http://www.ipb.ac.rs/~vrhovac/

TABLE I. Illustration of the construction of the objects larger than the basic ones for line segments, angled objects, and triangles. Here $n_s^{(x)}$ denotes the order of the symmetry axis of the shape. The ellipses denote objects larger than those shown explicitly.

Line segments $n_s = 2$		Angled objects $n_s = 1$		Triangles $n_s = 3$	
⊢—•	$\ell = 1$	⌐	$s = 1.5$	△	$s = 1$
•—•—•	$\ell = 2$	⌐	$s = 3$	◁	$s = 2$
...	...	...	...	...	...
...	$\ell = 10$	...	$s = 15$	...	$s = 5$

ferroelectric crystals, and dielectrics [20]. It has been shown that the Mittag-Leffler law (1) describes the relaxation of granular materials under very different modes of external excitation [21–23].

The relaxation dynamics of reversible deposition depends not only on the desorption to adsorption probability ratio but also on the order of symmetry of the shape and on the object size. Evolution of the coverage includes a rapid growth towards the jamming limit and a slow approach to the equilibrium coverage governed by collective adsorption-desorption events [24]. Namely, when θ_{jam} is reached, the rare desorption events are generally followed by immediate readsorption. These single-particle events do not change the total number of particles. However, when one badly sited object desorbs and two particles adsorb in the opened locations, the number of particles is increased by one. Likewise, if two well sited objects desorb and a single object adsorbs in their stead, the number of particles is decreased by one. Size of the objects and their symmetry properties have a significant influence on these collective events, thus affecting the kinetics of the process.

Particles in nature often vary in their size and shape so that polydispersity is an inevitable property in many experimental situations. Irreversible deposition of mixtures is studied in numerous works [25–28], but to the best of our knowledge there are very few works concerning adsorption-desorption processes of mixtures. Adsorption-desorption processes of polydisperse mixtures of hard disks on a continuous planar surface are studied in Ref. [29]. Results were obtained for various binding energies of the particles and a dramatic slowing down of the process was observed for the exponential decrease of the desorption rate with the particle size. It was found that the long time kinetics can be described with a stretched exponential function. The same kind of approach to the equilibrium was found for generalized RSA of polydisperse mixtures of k-mers on a one-dimensional lattice [18]. Reversible deposition of two-component mixtures on a triangular lattice is analyzed in Ref. [30]. Special attention was paid to the mixtures of objects of different shapes but covering the same number of lattice sites. Results show that kinetics of the adsorption-desorption process is considerably influenced by the order of symmetry of the shapes making the mixture.

Here we present the results of extensive simulations for the reversible RSA of polydisperse mixtures on a triangular lattice. The results are obtained by Monte Carlo simulations. The depositing objects are made by self-avoiding random walks on a two-dimensional (2D) triangular lattice. On a triangular lattice objects with a symmetry axis of first,

second, third, and sixth order can be formed. In the case of polydisperse mixtures we investigate the dependence of the deposition kinetics on the number of components in the mixture and on the length of the walks making the mixture, and we investigate the influence of the symmetry properties of depositing objects. We give the results not only for the whole mixture but also for the individual components.

II. DEFINITION OF THE MODEL AND THE SIMULATION METHOD

The polydisperse mixtures of extended objects on a 2D triangular lattice used in our simulations are shown in Tables I and II. Linear segments (k-mers) and angled objects that constitute the ten-component mixtures and triangles that constitute the five-component mixture of objects of various sizes are presented in Table I. In Table II three different shapes that can be made by self-avoiding walks of length $l = 2$ are shown. It should be noted that size s of an object is taken as the greatest projection of the walk that makes the object on one of the six directions. Thus the size of a dot is $s = 0$; the size of a one-step walk is $s = 1$; and, for example, the size of the first object in Table II is $s = 1.5$ in lattice spacing.

The Monte Carlo simulations are performed on a 2D triangular lattice of size $L = 120$. Periodic boundary conditions are used in all directions. The finite-size effects, which are generally weak, can be neglected for object sizes $< L/8$ [31].

At each Monte Carlo step a lattice site is selected at random and one of the objects making the mixture is selected at random, and we try to deposit the chosen shape of length l with probability P_a. If the selected site is occupied by a deposited object the adsorption attempt is rejected. If the selected site is unoccupied, we fix the beginning of the walk that makes the chosen shape at this site. Then we randomly pick one of the six possible orientations with equal probability, start the corresponding l-step walk in that direction, and search whether

TABLE II. (Color online) Various shapes (x) of length $\ell = 2$ on a triangular lattice. Here $n_s^{(x)}$ denotes the order of the symmetry axis of the shape.

(x)	Shape	$n_s^{(x)}$	$\ell^{(x)}$
(A)	•—•—•	2	
(B)	⌐	1	2
(C)	△	3	

all successive l sites are unoccupied. If so, we occupy these $l + 1$ sites and deposit the object; otherwise, the deposition attempt is rejected. Each adsorption attempt is followed by a desorption one with probability P_{des}. The desorption process starts by choosing a lattice site at random. If the selected site is unoccupied, the desorption step fails and the process continues by choosing a new site for the adsorption attempt. On the other hand, if the selected site is occupied by an adsorbed object, the object is removed from the lattice.

The reversible RSA process for a three-component mixture shown in Table II is as follows. From a large reservoir of shapes, which contains the shapes (A), (B), and (C) with the fractional concentrations $r^{(A)}$, $r^{(B)}$, and $r^{(C)}$, we choose one shape at random. The concentrations $r^{(A)}$, $r^{(B)}$, and $r^{(C)}$ are unaffected by adsorption or desorption events. We randomly select a lattice site and try to deposit the chosen shape with probability P_a in one of six orientations, which is randomly chosen. We fix the beginning of the walk that makes the shape at the selected site and search whether all successive l sites are unoccupied. If so, we occupy these $l + 1$ sites and place the object; otherwise the deposition attempt is rejected. When the attempted process is desorption, and the selected site is occupied by an object, the object is removed from the layer. In the reversible case, after a long enough time, the process reaches a steady state in which the rate of adsorption is exactly balanced by the rate of desorption.

It would be interesting to examine how the kinetics of the process is affected by the details of a desorption algorithm. We have performed some additional simulations using a different simulation algorithm in which an object is desorbed only if the beginning of the walk making the shape is at the selected site. In this case small and large objects desorb at the same rate.

The kinetics of the adsorption-desorption model depends only on the ratio P_{des}/P_a. In order to save the computer time t, it is convenient to take the adsorption probability to be $P_a = 1$, i.e., to try an adsorption at each Monte Carlo step. The time t is counted by the number of adsorption attempts and scaled by the total number of lattice sites L^2. The data are averaged over 1000 independent runs for each mixture of depositing objects and each desorption probability P_{des}.

III. RESULTS AND DISCUSSION

Simulations of the adsorption-desorption processes are performed for n-component mixtures ($n = 1, 2, \ldots, 10$) of linear segments (k-mers) and angled objects and for n-component mixtures ($n = 1, 2, \ldots, 5$) of triangles. For example, the two-component mixture of line segments consists of the lines of length $l = 1$ and $l = 2$, the three-component mixture is made by adding a line segment of length $l = 3$, and so on. An n-component mixture contains the lines of length $l = 1, 2, \ldots, n$ and all of them are adsorbed with equal probability. Mixtures of the other two shapes, i.e., angled objects and triangles, are made in a similar way.

Results are obtained for various low desorption probabilities in the range from $P_{des} = 0.0001$ to $P_{des} = 0.01$. Results for the time evolution of the partial and total coverages in the case of $P_{des} = 0.0001$ for the ten-component mixtures of line segments and angled objects are shown in Figs. 1(a) and 2(a), respectively, and results for the five-component mixture of
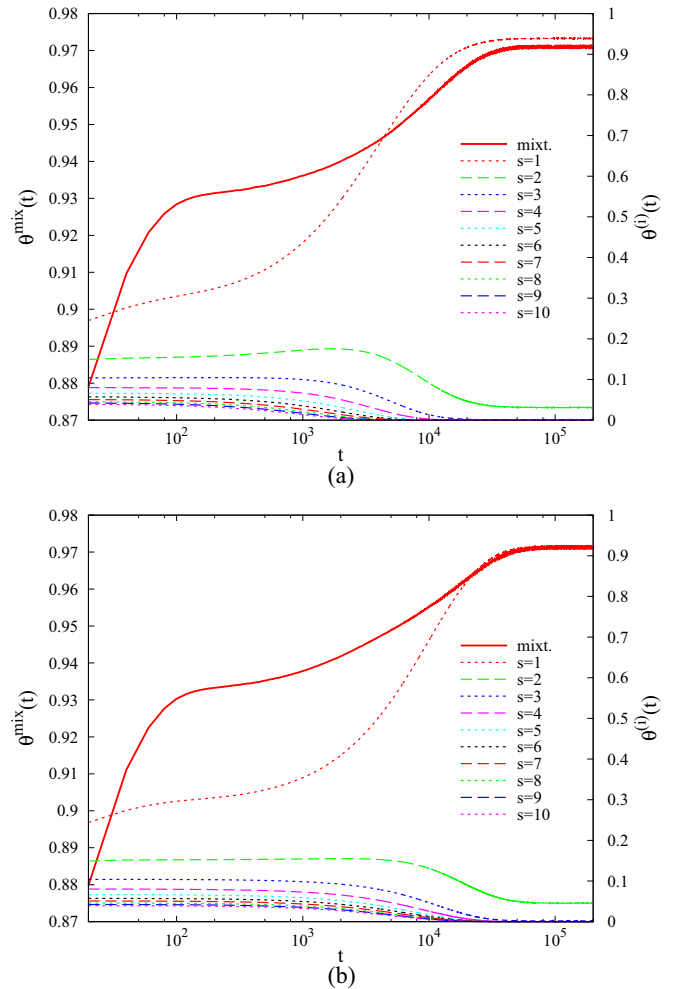

FIG. 1. (Color online) Time dependence of the partial coverages $\theta^{(i)}(t)$ for the ten-component mixture of line segments (right-hand axis) and the time dependence of the total coverage fraction $\theta^{mix}(t)$ (left-hand axis) for two different desorption algorithms. In the first algorithm the desorption attempt is successful if the selected site is occupied by an object (a), and in the second algorithm an object is desorbed if the beginning of the walk making the shape is at the selected site (b). Results shown in panels (a) and (b) are obtained for the same effective desorption probabilities for the smallest mixture component [$P_{des} = 0.0001$ in panel (a)].

triangles are shown in Fig. 3(a). Similar results are obtained for all desorption probabilities. From these figures we can see that only the time dependence of the partial coverage of the shortest objects is monotonically increasing. Partial coverage corresponding to any other component increases at the early times of the deposition process, reaches a maximum, and decreases slowly to its equilibrium value afterward. The contribution of longer objects to the total coverage becomes negligible for long times. Time evolution of the total coverage of a mixture is a two-stage process. At very early times of the process, when the coverage fraction is small, the adsorption process is dominant and the coverage grows rapidly in time. After this initial filling of the lattice, adsorption becomes slower and the desorption can no longer be ignored. Then, the change of the coverage requires the rearrangement of the
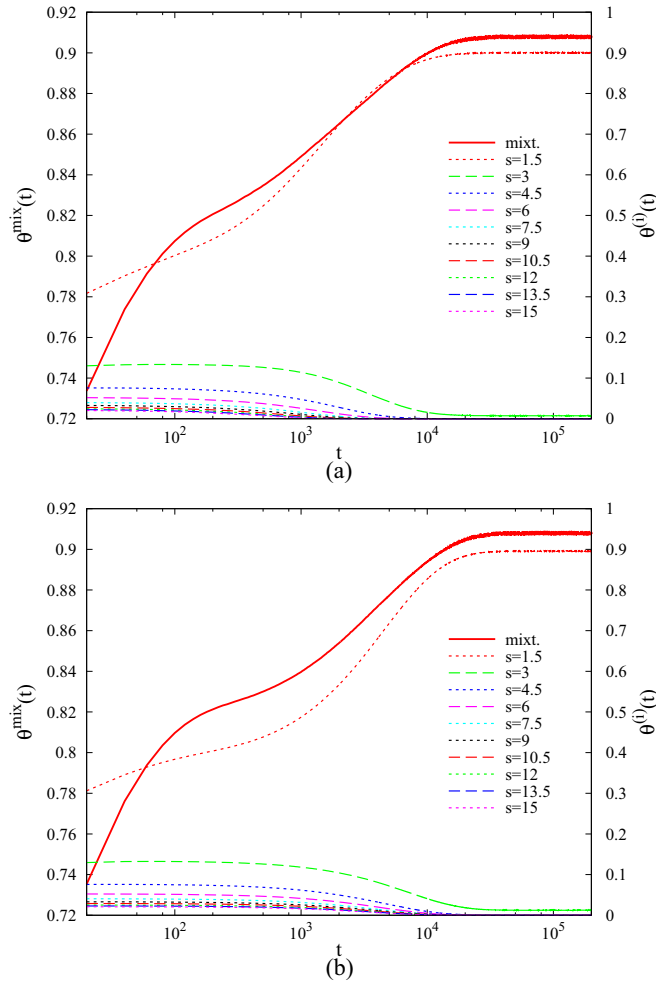
FIG. 2. (Color online) Time dependence of the partial coverages $\theta^{(i)}(t)$ for the ten-component mixture of angled objects (right-hand axis) and the time dependence of the total coverage fraction $\theta^{mix}(t)$ (left-hand axis) for two different desorption algorithms. In the first algorithm the desorption attempt is successful if the selected site is occupied by an object (a), and in the second algorithm an object is desorbed if the beginning of the walk making the shape is at the selected site (b). Results shown in panels (a) and (b) are obtained for the same effective desorption probabilities for the smallest mixture component [$P_{des} = 0.0001$ in panel (a)].
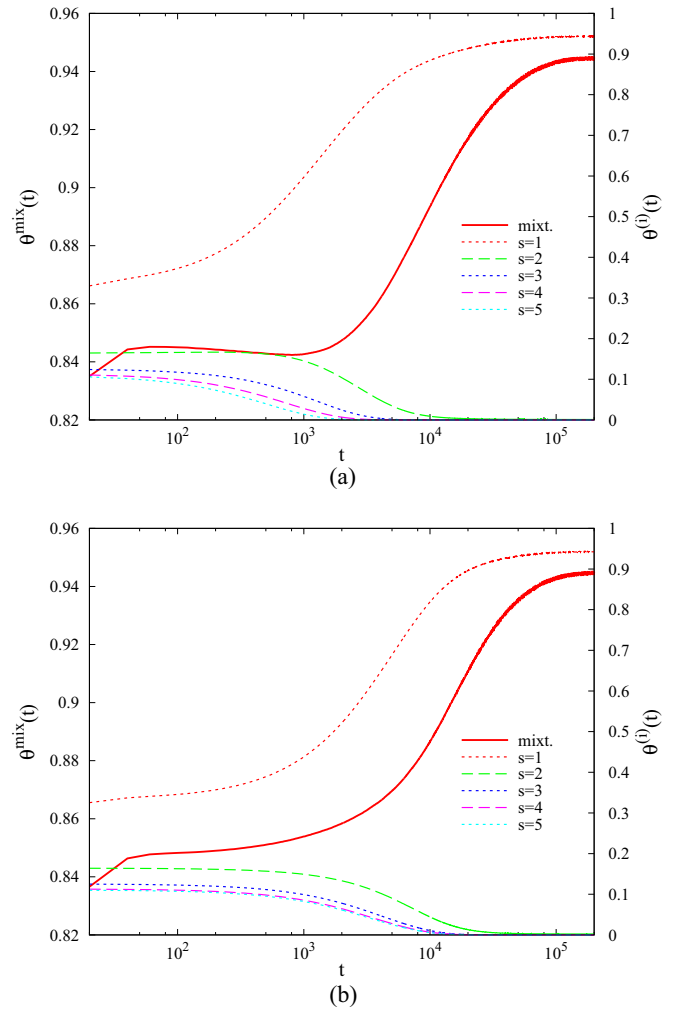
FIG. 3. (Color online) Time dependence of the partial coverages $\theta^{(i)}(t)$ for the five-component mixture of triangles (right-hand axis) and the time dependence of the total coverage fraction $\theta^{mix}(t)$ (left-hand axis) for two different desorption algorithms. In the first algorithm the desorption attempt is successful if the selected site is occupied by an object (a), and in the second algorithm an object is desorbed if the beginning of the walk making the shape is at the selected site (b). Results shown in panels (a) and (b) are obtained for the same effective desorption probabilities for the smallest mixture component [$P_{des} = 0.0001$ in panel (a)].

objects, which is caused by a long sequence of adsorption-desorption events in which an object detaches from the lattice and the gap that is created is immediately filled by one or more new objects. In this late stage, RSA acts to preferentially adsorb the shorter objects. This is a consequence of the fact that unlike for long objects, many more possible places for deposition are allowed for short objects falling into isolated empty locations. Therefore, the partial coverages of longer objects decrease in time. Fine-tuning of the incoming and outgoing flux of each component occurs during this stage. In the final regime, the coverage of the mixture increases due to the increase of the number of the shortest objects in the layer.

Results obtained using the desorption algorithm in which an object is removed from the lattice only if the beginning of the object is at the selected site are shown in Figs. 1(b), 2(b), and 3(b) for the ten-component mixture of line segments,

the ten-component mixture of angled objects, and the five-component mixture of triangles, respectively. Desorption probabilities are chosen to be the same as the effective desorption probabilities for the smallest mixture components in Figs. 1(a), 2(a), and 3(a). Comparing the graphs (a) and (b), obtained using the two different desorption algorithms, we can see that the approach to the equilibrium slows down when the desorption probability of larger objects decreases. However, regardless of the details of the algorithm, only the partial coverage of the smallest object in the mixture monotonically increases. The qualitative time dependence of larger objects' partial coverage also remains unchanged. Furthermore, the values of the equilibrium coverage for the mixture, as well as the equilibrium coverages of the mixture components, are practically not affected by this change in the desorption algorithm.
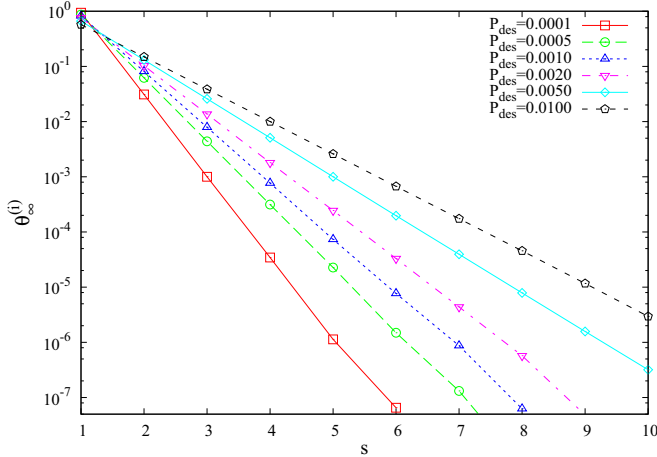
FIG. 4. (Color online) Dependence of the partial steady-state coverage on the size s of the objects for the ten-component mixture of line segments. The error bars for the steady-state coverages are smaller than the symbol size.

Dependence of the partial steady-state coverage on the size of the objects for the ten-component mixture of line segments is shown in Fig. 4 for various desorption probabilities. It can be seen that the presence of longer objects becomes negligible in the final stage of the process. Similar graphs are obtained for the ten-component mixture of angled objects and for the five-component mixture of triangles. The reasons for these results are intuitively clear. Due to the fact that the densification kinetics is dictated by geometric exclusion effects, in the competition for adsorption between different objects, the smaller objects win. As expected, for all these mixtures, partial steady-state coverage of the smallest component is higher for lower probabilities. Increasing the desorption probability enhances the contribution of the larger objects from the mixture due to the geometric exclusion effects.

We have found that above the jamming limit, the time evolution of the total coverage of the mixture can be described by Eq. (1). Here values of the steady-state coverage θ_∞, the parameter $\Delta\theta$, and the relaxation time τ depend on the desorption probability $P_{\rm des}$ and on the mixture composition. In Figs. 5–7 the results of the simulations are shown together with the fits of Eq. (1) for two different mixtures of line segments, angled objects, and triangles, respectively. We can see that the Mittag-Leffler fitting function shows a very good agreement with the simulation results in the region above the jamming limit. The fitting values of the parameter τ show that the relaxation time increases when the desorption probability decreases, for all types of mixtures; i.e., the process is slower for lower values of $P_{\rm des}$. Comparing the values of relaxation time τ for mixtures of line segments, angled objects, and triangles, with equal numbers of components, we can see that the mixtures of triangles have the largest values of relaxation time and the mixtures of angled objects have the smallest values of relaxation time. This is in agreement with the results for the monodisperse deposition [10], according to which the dynamical behavior is severely slowed down with the increase of the order of symmetry of the shape. Symmetry properties of the shapes have a great influence in the later times of the deposition process. Namely, in the late stages of
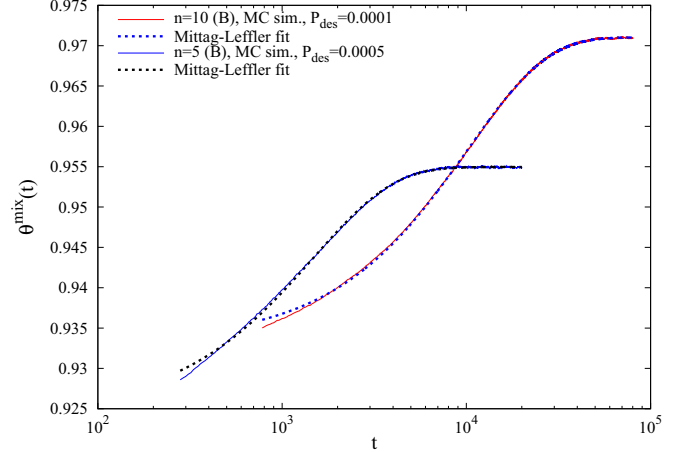

FIG. 5. (Color online) Temporal behavior of the coverage $\theta(t)$ for the ten-component mixture of line segments for $P_{\rm des} = 0.0001$ [gray (red) line] and for the five-component mixture of line segments for $P_{\rm des} = 0.0005$ [black (blue) line]. The dashed curves are the Mittag-Leffler fits of Eq. (1).

the adsorption-desorption processes, the rare desorption events are generally followed by immediate readsorption. The total number of particles is not changed by these single-particle events. However, when one badly sited object desorbs and two particles adsorb in the opened good locations, the number of particles is increased by one ("$1 \rightarrow 2$"). Likewise, if two well-sited objects desorb and a single object adsorbs in their stead, the number of particles is decreased by one ("$2 \rightarrow 1$"). The steady-state is reached when the rate of the former process is balanced by the rate of the latter one. A shape with a symmetry axis of higher order has a greater number of possible orientations for deposition into small isolated locations on the lattice and, therefore, enhanced probability of single-particle readsorption. This extends the mean waiting time between consecutive two-particle events $1 \rightarrow 2$, responsible for the
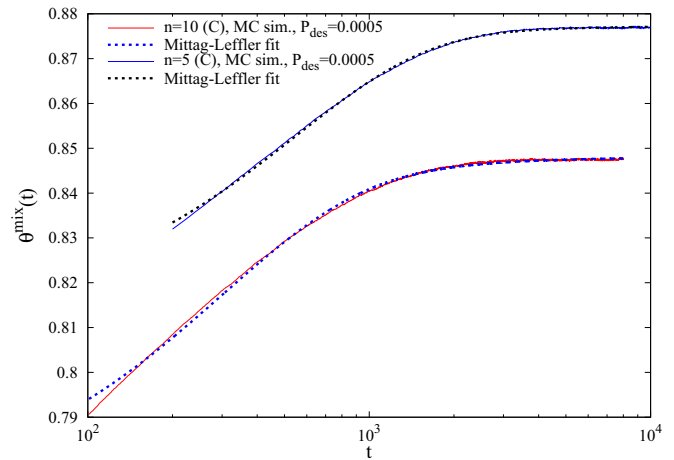

FIG. 6. (Color online) Temporal behavior of the coverage $\theta(t)$ for the ten-component mixture of angled objects [gray (red) line] and the five-component mixture of angled objects [black (blue) line]. All the results are for $P_{\rm des} = 0.0005$. The dashed curves are the Mittag-Leffler fits of Eq. (1).
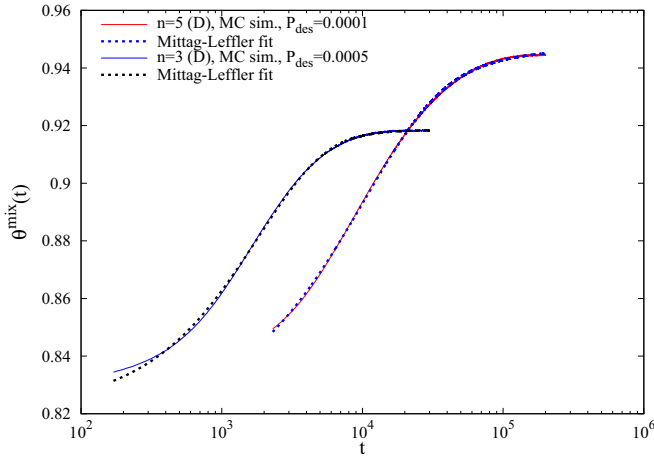
FIG. 7. (Color online) Temporal behavior of the coverage $\theta(t)$ for the five-component mixture of triangles for $P_{\text{des}} = 0.0001$ [grey (red) line] and for the three-component mixture of triangles for $P_{\text{des}} = 0.0005$ [black (blue) line]. The dashed curves are the Mittag-Leffler fits of Eq. (1).

density growth above θ_{jam}, and causes a slowing down of the densification.

Dependence of the steady-state coverage of the deposition process on the number of components in the mixture is also studied. The results for θ_{∞} are shown for the mixture of line segments in Fig. 8 for various desorption probabilities. Qualitatively similar dependence is obtained for the mixtures of angled objects and for the mixtures of triangles. Figure 8 shows that the steady-state coverage decreases with the number of components in the mixture according to a stretched exponential law:

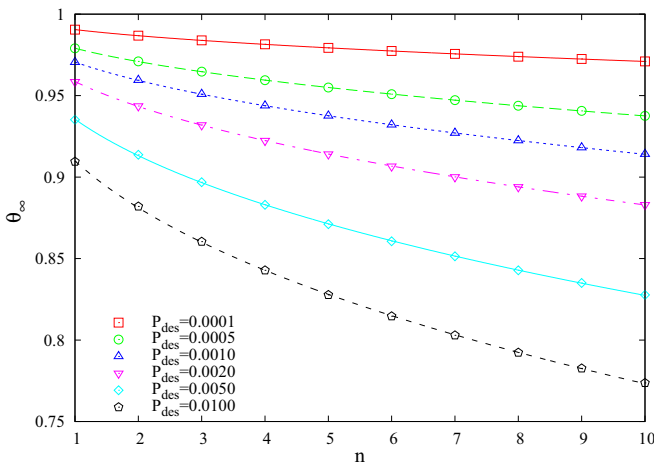$$\theta_{\infty} = \theta_0 \exp[-(n/\alpha)^{\beta}], \quad (2)$$

FIG. 8. (Color online) Dependence of the partial steady-state coverage on the number of components for the mixture of line segments. The number of components n in the mixture is always increased by adding an object of a greater size. Here the error bars do not exceed the size of the symbols. The lines are fits of the stretched exponential function: $\theta_{\infty} = \theta_0 \exp[-(n/\alpha)^{\beta}]$.
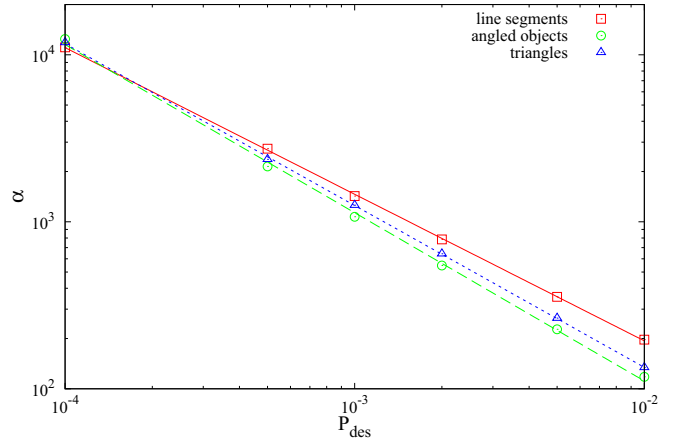

FIG. 9. (Color online) Parameter α of the stretched exponential fit of Eq. (2) vs the desorption probability P_{des} for the mixtures of line segments, angled objects, and triangles.

where θ_0, α, and β are the fitting parameters. Figure 9 shows the dependence of the parameter α on desorption probabilities for the studied mixtures. Parameter β is in the range of 0.3–0.5 for all types of mixtures.

Plots of the total equilibrium coverage against the desorption probability are shown for the n-component mixtures ($n = 1, 2, \ldots, 10$) of linear segments in Fig. 10(a), for the n-component mixtures ($n = 1, 2, \ldots, 10$) of angled objects in Fig. 10(b), and for the n-component mixtures ($n = 1, 2, \ldots, 5$) of triangles in Fig. 10(c). From Fig. 10 we can see that decrease of the steady-state coverages occurs via a stretched exponential law of the form

$$\theta_{\infty} = \theta_0 \exp[-(P_{\text{des}}/\gamma)^{\delta}], \quad (3)$$

where θ_0, γ, and δ are the fitting parameters. Dependence of the parameter γ on the number of components n is shown in Fig. 11, for the mixtures of line segments, angled objects, and triangles. Parameter δ is in the range from 0.3 to 0.5 for all types of mixtures.

We have also performed numerical simulations of adsorption-desorption processes for the three-component mixture of various shapes, shown in Table II. These shapes are made of self-avoiding walks of the same length $l = 2$, but they differ in their symmetry properties. The results for the time evolution of the partial and total coverages in the case of $P_{\text{des}} = 0.0005$ are shown in Fig. 12. Similar results are obtained for all desorption probabilities. Figure 12 shows that the partial coverages of the shapes of higher order of symmetry ($n_s^{(C)} = 3$; $n_s^{(A)} = 2$) are monotonously increasing functions of time and have the same general features as the coverage for mixture. On the other hand, the partial coverage of the shape (B) of the lowest order of symmetry ($n_s^{(B)} = 1$) is not monotonic in time. When the coverage of the mixture approaches the jamming limit $\theta_{\text{jam}} = 0.877$, the coverage of the shape (B) reaches a maximum, which is followed by a slow relaxation to the smaller steady-state value. Results of the simulations show that a larger value for the maximum of the coverage $\theta^{(B)}(t)$ is reached for smaller desorption probability and that the maximum of $\theta^{(B)}(t)$ shifts towards longer times as the desorption probability decreases. It is also obvious that the steady-state
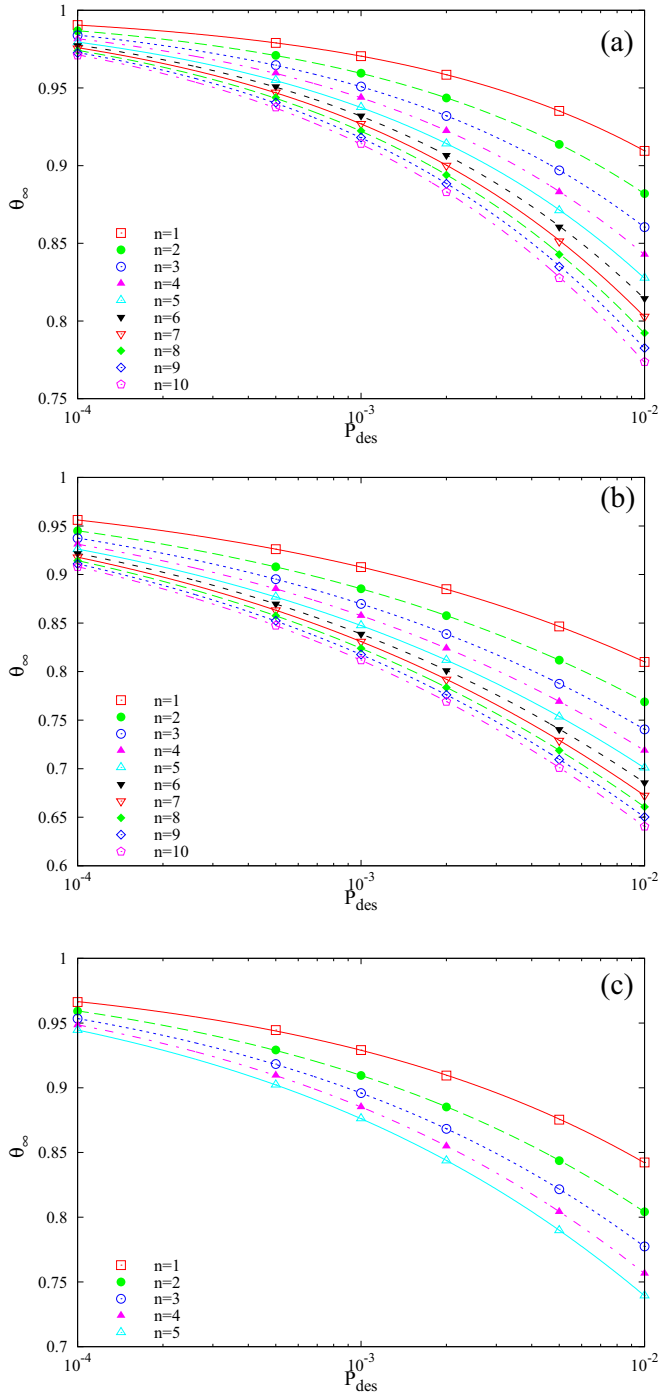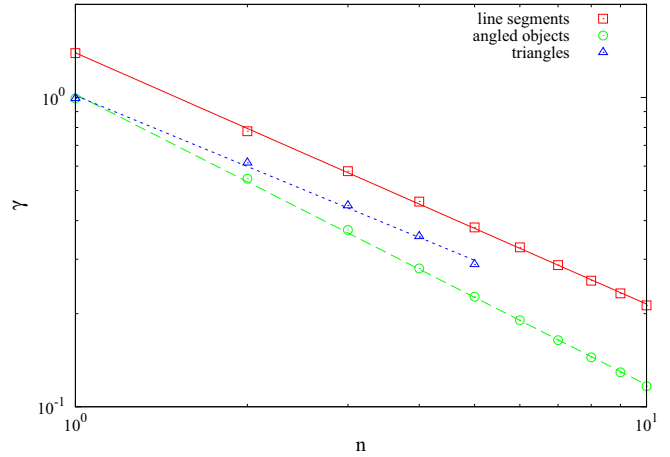
FIG. 11. (Color online) Parameter γ of the stretched exponential fit of Eq. (3) vs the number of components n for the mixtures of line segments, angled objects, and triangles.

unoccupied sites. The symmetry properties of the shapes have a significant influence on the filling of small isolated locations on the lattice. Indeed, there is only a restricted number of possible orientations in which an object can reach a previously opened location, provided that location is small enough. For the more symmetric shapes there are a greater number of possible orientations for deposition into an isolated location on the lattice. The adsorption of asymmetric shapes is less efficient than the adsorption of more regular and symmetric shapes. This is reflected in the gradual decrease of the coverage fraction with time for the shape with the symmetry axis of the lowest order.

From Fig. 12 we can see that the steady-state value of the total coverage of the mixture was reached before the partial coverages of the components achieved their steady-state values. The coverage fraction of the mixture fluctuates around its steady-state value, while the coverage fractions of the more

FIG. 10. (Color online) Dependence of the total steady-state coverages on the desorption probability P_{des} for the n-component mixtures of (a) line segments, (b) angled objects, and (c) triangles. The lines are fits of the stretched exponential function: $\theta_\infty = \theta_0 \exp[-(P_{des}/\gamma)^\delta]$.

value of the partial coverage fraction is always larger for the shapes with a symmetry axis of higher order. The presented results suggest that at late enough times, when the coverage fraction is sufficient to make the geometry of the unoccupied sites complex, there is a strong dependence of the adsorption rate on the shape of the adsorbing objects [7,10,30]. At long times, adsorption events take place on isolated islands of connected
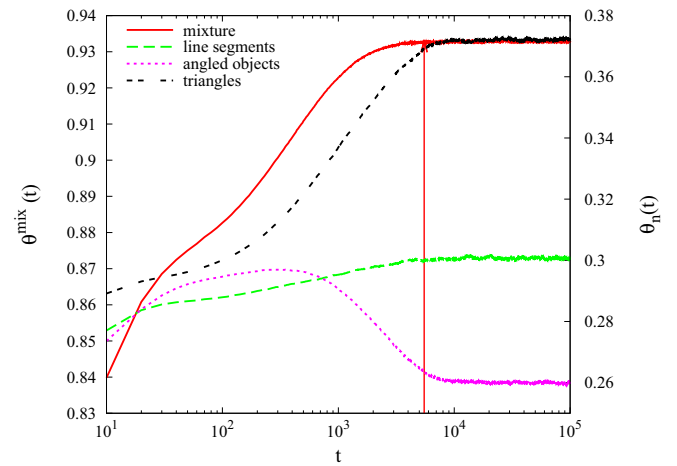

FIG. 12. (Color online) Time dependences of the partial coverages $\theta_n(t)$ for the three-component mixture of line segments, angled objects, and triangles (right-hand axis) and the time dependence of the total coverage fraction $\theta^{mix}(t)$ (left-hand axis) for the same mixture. All the results are for $P_{des} = 0.0005$ and for fractional concentrations that are in proportion $r^{(A)} : r^{(B)} : r^{(C)} = 1:1:1$.
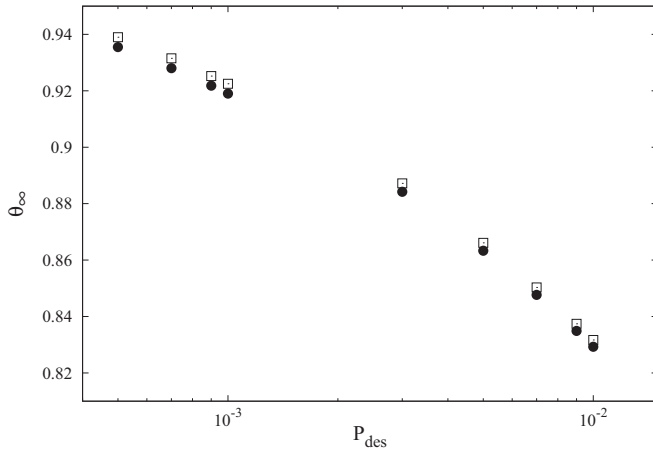
FIG. 13. Plot of the steady-state coverage fraction $\theta_\infty^{(A)+(B)+(C)}$ against the desorption probability P_{des} for fractional concentrations that stand in proportion $r^{(A)} : r^{(B)} : r^{(C)} = 1{:}5{:}10$. Closed symbols refer to the data obtained from the numerical simulations. Open symbol are the steady-state coverages $\theta_\infty^{(A)+(B)+(C)}$ calculated from Eq. (4).

symmetric shapes continue to grow at the expense of the coverage fraction of the component with the symmetry axis of the lowest order, which decreases. In the late stage of the process RSA acts to preferentially adsorb the more regular shapes from the reservoir, but higher values of their coverage fractions enhance the frequencies of desorption events. Moreover, the least symmetric shape adsorbs less efficiently, but a lower value of its coverage fraction decreases the frequency of desorption events. The presence of the above-described mechanism implies that each mixture component reaches a steady state.

Recently, we have proposed a simple formula for calculating the steady-state fraction $\theta_\infty^{(x)+(y)}$ in the binary mixture $(x) + (y)$ of equal-sized shapes (x) and (y) with fractional concentrations $r^{(x)}$ and $r^{(y)}$ in an infinite reservoir [30]. We have carried out extensive simulations of reversible RSA for the three-component mixture of shapes shown in Table II for various fractional concentrations, in order to see whether a similar formula can be used to predict the value of the steady-state coverage fraction of a mixture from the values of the steady-state coverage fractions of pure component shapes. We propose the following formula:

$$\frac{1}{\theta_\infty^{(A)+(B)+(C)}} = r^{(A)}\frac{1}{\theta_\infty^{(A)}} + r^{(B)}\frac{1}{\theta_\infty^{(B)}} + r^{(C)}\frac{1}{\theta_\infty^{(C)}}, \qquad (4)$$

where $\theta_\infty^{(A)}$, $\theta_\infty^{(B)}$, and $\theta_\infty^{(C)}$ are the steady-state coverage fractions of the pure lattice shapes and $r^{(A)}$, $r^{(B)}$, and $r^{(C)}$ are their fractional concentrations in the reservoir.

Formula (4) is supported by good agreement with the numerical simulations. Figure 13 compares the steady-state coverage fraction $\theta_\infty^{(A)+(B)+(C)}$ as a function of desorption probability P_{des} with the values obtained using Eq. (4). Objects are deposited from the reservoir that contains the shapes (A), (B), and (C) with fractional concentrations $r^{(A)}$, $r^{(B)}$, and $r^{(C)}$, which stand in proportion 1:5:10. One clearly observes that Eq. (4) very well predicts the values of $\theta_\infty^{(A)+(B)+(C)}$ from the values of the steady-state coverage fraction of pure component shapes, in the whole range of desorption

probability P_{des} considered. Similar agreement is confirmed for various combinations of fractional concentrations.

IV. CONCLUDING REMARKS

We have studied the reversible RSA of polydisperse mixtures on a triangular lattice by numerical simulations. Mixtures were composed of shapes of different numbers of segments and rotational symmetries. It was shown that the coverage kinetics of a mixture has a richer behavior in comparison to that of the reversible deposition of pure lattice objects. In the case of mixtures in which components differ in size, it turned out that only the time dependence of the smallest objects is monotonically increasing. Partial coverage of any other component increases at the early times of the deposition process, reaches a maximum, and decreases to its equilibrium value as a result of the interplay between the incoming and the outgoing flux of each mixture component. The contribution of longer objects to the total coverage becomes negligible in the late times of the process. Such deposition kinetics gives a good qualitative description of the segregation process in polydisperse granular materials under vertical tapping.

Despite the complexity of the adsorption-desorption processes of polydisperse mixtures, above the jamming limit, the time evolution of the total coverage of a mixture can be described by the Mittag-Leffler function for all the mixtures we have examined. The same type of approach to the steady-state coverage has been found for the adsorption-desorption processes of monodisperse objects on a triangular lattice [10].

Simulations were performed for various numbers of components making the mixture and for various desorption probabilities. The number of components was increased by adding an object of a greater length. It was found that the equilibrium coverage decreases with the number of components making the mixture and also with the desorption probability, via corresponding stretched exponential laws.

Special attention has been paid to the mixtures containing objects of various shapes, but made of the same number of segments. It was found that the coverage kinetics of a mixture strongly depends on the symmetry properties of the component shapes. For sufficiently long times, the coverage fraction of more symmetric shapes exceeds the coverage fraction of less symmetric ones. After the total coverage of the mixture reaches its steady-state value, the partial coverages of more symmetric components continue to grow, while the coverage fraction of the least symmetric object decreases until they all achieve their steady-state values. We have proposed a simple formula (4) that can be used to predict the value of a steady-state coverage fraction of a mixture knowing the steady-state coverage fractions of the pure component shapes. Such a formula could be used to avoid the time-consuming simulations of the reversible RSA of mixtures.

[1] J. W. Evans, Rev. Mod. Phys. **65**, 1281 (1993).

[2] V. Privman, Colloids Surf., A **165**, 231 (2000).

[3] A. Cadilhe, N. A. M. Araujo, and V. Privman, J. Phys.: Condens. Matter **19**, 065124 (2007).

[4] B. Bonnier, Phys. Rev. E **64**, 066111 (2001).

[5] D. J. Burridge and Y. Mao, Phys. Rev. E **69**, 037102 (2004).

[6] M. C. Bartelt and V. Privman, J. Chem. Phys. **93**, 6820 (1990).

[7] Lj. Budinski-Petković and U. Kozmidis-Luburuć, Phys. Rev. E **56**, 6904 (1997).

[8] E. Frey and A. Vilfan, Chem. Phys. **284**, 287 (2002).

[9] J. Talbot, G. Tarjus, and P. Viot, Phys. Rev. E **61**, 5429 (2000).

[10] Lj. Budinski-Petković, M. Petković, Z. M. Jakšić, and S. B. Vrhovac, Phys. Rev. E **72**, 046118 (2005).

[11] G. Tarjus and P. Viot, Phys. Rev. E **69**, 011307 (2004).

[12] Lj. Budinski-Petković and S. B. Vrhovac, Eur. Phys. J. E **16**, 89 (2005).

[13] P. L. Krapivsky and E. Ben-Naim, J. Chem. Phys. **100**, 6778 (1994).

[14] J. Talbot, G. Tarjus, and P. Viot, J. Phys. A: Math. Gen. **32**, 2997 (1999).

[15] X. Jin, G. Tarjus, and J. Talbot, J. Phys. A: Math. Gen. **27**, L195 (1994)

[16] P. Ranjith and J. F. Marko, Phys. Rev. E **74**, 041602 (2006).

[17] I. Lončarević, Lj. Budinski-Petković, S. B. Vrhovac, and A. Belić, Phys. Rev. E **80**, 021115 (2009).

[18] I. Lončarević, Lj. Budinski-Petković, S. B. Vrhovac, and A. Belić, J. Stat. Mech. (2010) P02022.

[19] R. K. Saxena, A. M. Mathai, and H. J. Haubold, Phys. A (Amsterdam, Neth.) **344**, 657 (2004).

[20] R. Hilfer, J. Non-Cryst. Solids **305**, 122 (2002).

[21] W. L. Vargas and J. J. McCarthy, Phys. Rev. E **76**, 041301 (2007).

[22] T. Divoux, H. Gayvallet, and J.-C. Geminard, Phys. Rev. Lett. **101**, 148303 (2008).

[23] N. Mueggenburg, Phys. Rev. E **85**, 041305 (2012).

[24] R. S. Ghaskadvi and M. Dennin, Phys. Rev. E **61**, 1232 (2000).

[25] M. Henkel and N. M. Švrakić, J. Phys. I **1**, 791 (1991).

[26] G. Tarjus and J. Talbot, Phys. Rev. A **45**, 4162 (1992).

[27] Z. Adamczyk, B. Siwek, M. Zembala, and P. Weronski, J. Colloid Interface Sci. **185**, 236 (1997).

[28] Lj. Budinski-Petković, S. B. Vrhovac, and I. Lončarević, Phys. Rev. E **78**, 061603 (2008).

[29] C. B. Olson and J. Talbot, J. Chem. Phys. **112**, 3868 (2000).

[30] I. Lončarević, Lj. Budinski-Petković, and S. B. Vrhovac, Phys. Rev. E **76**, 031104 (2007).

[31] S. S. Manna and N. M. Švrakić, J. Phys. A **24**, L671 (1991).